Challenges and Perspectives on Impulse Radio-Ultra-Wideband Transceivers for Neural Recording Applications

Razieh Eskandari and Mohamad Sawan

***Abstract*—Brain-machine interfaces (BMI) are widely adopted in neuroscience investigations and neural prosthetics, with sensing channel counts constantly increasing. These Investigations place increasing demands for high data rates and low-power implantable devices despite high tissue losses. The Impulse radio ultra-wideband (IR-UWB), a revived wireless technology for short-range radios, has been widely used in various applications. Since the requirements and solutions are application-oriented, in this review paper we focus on neural recording implants with high-data rates and ultra-low power requirements. We examine in detail the working principle, design methodology, performance, and implementations of different architectures of IR-UWB transceivers in a quantitative manner to draw a deep comparison and extract the bottlenecks and possible solutions concerning the dedicated application. Our analysis shows that current solutions rely on enhanced or combined modulation techniques to improve link margin. An in-depth study of prior-art publications that achieved Gbps data rates concludes that edge-combination architecture and non-coherent detectors are remarkable for transmitter and receiver, respectively. Although the aim to minimize power and improve data rate - defined as energy efficiency (pJ/b) - extending communication distance despite high tissue losses and limited power budget, good narrow-band interference (NBI) tolerance coexisted in the same frequency band of UWB systems, and compatibility with energy harvesting designs are among the critical challenges remained unsolved. Furthermore, we expect that the combination of artificial intelligence (AI) and the inherent advantages of UWB radios will pave the way for future improvements in BMIs.**

***Index Terms*—Brain-machine interface (BMI), Carrier-less transmitter, Edge-combination architecture, Energy detector, Envelope detector, High data rate, Impulse Radio ultra-wideband (IR-UWB) transceiver, Neural Recording Implants, Non-Coherent receivers, Ultra-low power.**

I. Introduction

OUR knowledge of the nervous system is bounded by how precisely the activity of groups of neurons can be measured. Since technical constraints, the simultaneous recording had limited to only a few cells for some time. The relatively slow rate of neurotechnology development can be attributed to several factors, such as the lack of industrial support, difficulties in scaling electrodes to increase sampling volume, tissue safety concerns, challenges in developing input/output (I/O) interfaces, and the need for efficient energy sources for implants.

The authors are with the Center of Excellence in Biomedical Research on Advances-on-Chips Neuro technologies (CenBRAIN Neurotech) School of Engineering, Westlake University, Hangzhou 310024, China (email: r.eskandari@westlake.edu.cn, sawan@westlake.edu.cn)

Manuscript received XXX

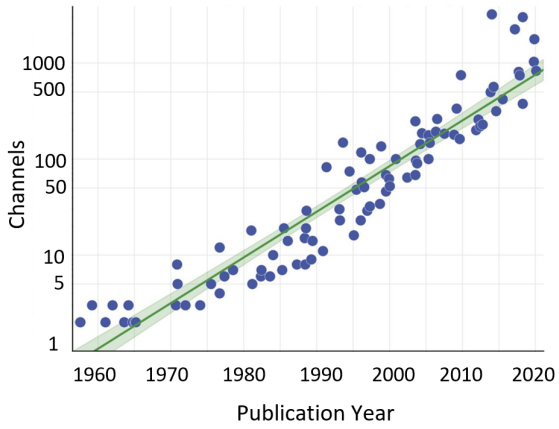

Fig. 1. Exponential growth in simultaneous recording channels [2].

The progress in neural recording technologies over the past few decades has been remarkable, with exponential growth in the number of simultaneous recording channels doubling every seven years, as was first revealed by [1], Fig. 1 [2]. However, comparing this trend with the number of all brain neurons, which is almost 100 million for mice and close to 100 billion for humans, confirms that we are still in the early stages of understanding brain and animal behavior comprehensively. The increasing demand for low-power and short-range wireless communications has led to the development of several narrow-band solutions, such as IEEE 802.15.4, Bluetooth Low Energy (BLE), ISM band, and Medical Device Radio Communications Service (MedRadio)[3]–[8]. Despite their low power performance and low tissue losses, these radios are unlikely to satisfy the constraints of upcoming multi-brain-machine interfaces (BMI) with thousands of recording channels, including small area, severe power budget, heat dissipation, and high data rates [9][10]. IR-UWB solutions, which offer a wide transmission bandwidth and high energy efficiency, are good candidates for achieving higher data throughput. The Federal Communication Commission (FCC) classifies a signal as UWB if the bandwidth (BW) is wider than either 500 MHz or wider than 0.2 times carrier frequency [11].

Since UWB signals occupy a wide frequency band in which other narrow-band transceivers are also present, the maximum power spectrum density (PSD) is restricted to -41 dBm for noise integration BW of 1 MHz. To prevent interference with other radios, the allowed power levels vary for frequency

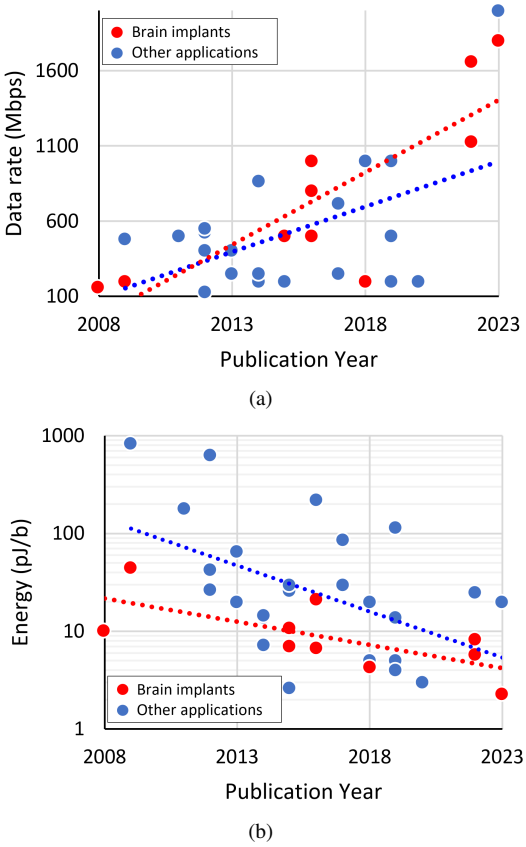

Fig. 2. racking the Evolution of a) Data Rate, and b) Energy Consumption in high-throughput IR-UWB transceivers for brain implants vs. other applications over the last 15 years.

ranges below 3.1 GHz.

Fig. 2 (a) shows the trend in data rate for IR-UWB transceivers over the last 15 years in publications reporting data rates above 100 Mbps. Fig. 2 (b) illustrates the energy (pJ/b) consumption to evaluate the power budget per bit in these reports. The trend of data rate enhancement and power reduction reflects the continued efforts made in recent years to improve the performance of UWB transceivers in all applications. However, neural recording applications present a faster growth in data rate to address the stringent requirements of emerging BMIs with thousands of recording channels. Regarding energy, all applications have started to reduce power while for neural implants power has been a persistent concern. Over the years, significant efforts have been made to address this issue and downward trend has continued.

The UWB transmitters can be classified as carrier-less and carrier-based architectures, each consisting of three fundamental functions: narrow pulse generation, frequency synthesis, and power amplification. Numerous modulation schemes, such as On-Off-Keying (OOK), Pulse Amplitude Modulation (PAM), Binary Phase Modulation (BPM), Pulse Width Modulation (PWM), and Pulse Position Modulation (PPM) can be utilized. The narrow pulses in the pulse generation block modulate the RF signal to achieve a wide spectrum. Such narrow pulse radios offer promising features. Firstly, the short duty cycle reduces power consumption [12] through periodic operation, which is essential for ultra-low power applications and avoiding tissue heating. Propagation, absorption rate, and temperature analysis of IR-UWB implants in the human body are studied at [13]–[15]. Secondly, it provides high resolution in both time and space domains required in applications with high accuracy [16]–[18]. To demonstrate remarkable accuracy in UWB technology, [19] and [20] achieved the ranging accuracy of 3.75 cm and 2.5 mm, respectively. Typical IR-UWB transceivers with reported data rates in the range of a few Mbps can meet the requirements for medical applications like optical imaging, retinal prosthetic implants, and wireless biomedical sensors. However, the major challenge is to achieve higher data rates with a more restricted power budget for brain implants, where energy is provided by energy harvesting, wireless power link through inductive coupling, or lightweight and small batteries.

The UWB signal emitted from the source passes through multiple layers of tissue before it reaches the receiving antenna for detection. Most studies have relied on either simulation models or experiments with biological-equivalent phantoms. The attenuation of a living body in UWB transmission performance is studied in [21]–[23] to present a realistic model of biomedical communication channels. The low signal-to-noise ratio (SNR) channel, besides the low-duty-cycle nature of UWB radios poses a significant challenge for achieving synchronization between a transmitter and a receiver. Another concern is to extend the communication range to facilitate reliable experiments on freely behaving patients/animals. Among the different receivers, coherent architectures provide the optimum solution for robust performance with precise synchronization demands [24], [25] at the expense of high power budget. Non-coherent alternatives, such as energy detectors, have gained more interest due to their low complexity and low power features [26]–[29].

This review paper analyzes the research efforts in IR-UWB transceivers, architectures, and building blocks in a quantitative manner to draw a deep comparison and identify the bottlenecks and possible solutions. Given the specific restrictions and design challenges posed by brain-machine interfaces, this study delves into the structures and improvements specific to this dedicated application. Section II of this review outlines the IR-UWB transmitter architectures, classifications, and building blocks. IR-UWB receivers are introduced in section III, further improvement and future trends are presented in section IV, followed by a conclusion in section V.

II. TRANSMITTER

Among different approaches for IR-UWB transmitters, they can be divided into carrier-less and carrier-based topologies. The former approach is based on Gaussian waveforms or their derivative, while the latter one employs an oscillator to generate the carrier of UWB pulses. The evaluation criteria of IR-UWB transceivers consist of power consumption, data rate, energy efficiency, radio range, die area, heat dissipation, etc. To make a general view around both architectures, Fig. 3 plots FOM as a function of data rate in both IR-UWB transmitters in recent papers. The comparison metric (FOM)

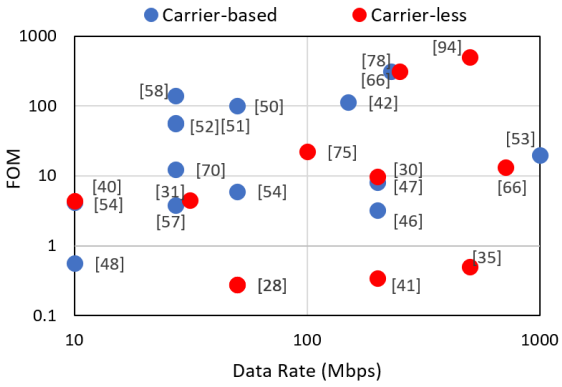

Fig. 3. Comparison of carrier-less and carrier-based architectures in recent reports.

for a holistic evaluation is defined as Eq.(1) [30], [31]. The prevalence of reports indicating data rates exceeding 10 Mbps and FOM values below 1 strongly suggests that the carrier-less structure holds significant promise for achieving high data rates and efficient transmission. This underscores the potential advantages of utilizing a carrier-less approach, enabling more effective use of available bandwidth and better system performance overall.

$$FOM = \frac{Area(mm^2)Energy(pJ/b)}{V_{(p-p)}(V)} \tag{1}$$

In the subsequent sections, a comprehensive overview of both techniques is presented, with a particular emphasis on highlighting the unique features and innovations associated with each approach.

A. Carrier-Less architecture

Typical carrier-free or edge-combining IR-UWB transmitters generate narrow pulses at the baseband and convert them to UWB RF signals. Avoiding the need for up-conversion mixers results in a simple structure and low power consumption [29], [32]. Furthermore, this design supports both BPSK and OOK modulation schemes, providing flexibility in managing the power budget trade-off with the desired bit error rate (BER) performance. For a Gaussian function (Eq.2), the n^{th} derivative Gaussian pulse, Fourier transform, and center frequency are expressed as [33], [34]:

$$g(t) = \pm\frac{A\sqrt{2}}{\alpha} \times e^{\frac{-2\pi t^2}{\alpha^2}} \tag{2}$$

$$g^{(n)}(t) = -\frac{4\pi(n-1)}{\alpha^2}g^{(n-2)}(t) - \frac{4\pi t}{\alpha^2}g^{(n-1)}(t) \tag{3}$$

$$G_n(f) = A(j2\pi f)^n \times e^{\frac{-\pi(\alpha f)^2}{2}} \tag{4}$$

$$f_{peak}(GHz) = \sqrt{n}\frac{1}{\alpha\sqrt{n}} \tag{5}$$

where A represents the pulse amplitude, t is time, and α is the pulse shaping factor. The pulse shaping parameters for the UWB transmission are mathematically analyzed in [34] and shown that n and α should be selected jointly based on the center frequency and -3dB bandwidth requirements.

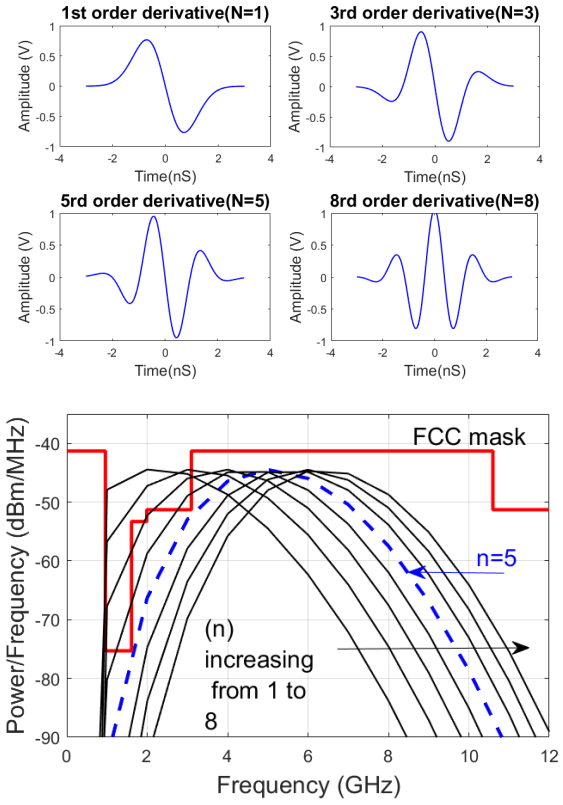

Fig. 4. Different derivatives of Gaussian wavelets and their spectral profile.

Fig. 4 shows the MATLAB simulation of Gaussian derivation pulses and their corresponding frequency spectra while n is increasing from 1 to 8. Although mono pulses are desirable due to simple and low power implementation, they do not fit the mask and demand a power-hungry frequency shifter or an area-expensive filter to shape the output spectrum [32]. In contrast, the higher-order derivatives of the Gaussian pulse resemble sinusoids modulated by a Gaussian pulse-shaped envelope, which shifts the center frequency to fit the spectrum to the given regulation [35]. This feature makes higher-order derivatives of the Gaussian pulse the better candidates for UWB transmission [30], [33], [36]–[38]. Simulations in Fig. 4 confirms that a Gaussian pulse with at least a fifth derivative (n=5) is required to satisfy the FCC mask. Since the higher and the lower sidelobes of the PSD are not symmetrically scaled with n and α, choosing the proper value for these parameters is not easy in multi-band allocations. Therefore, it is difficult to allocate adjacent bands without interference[39], [40].

Fig. 5 illustrates two common architectures for carrier-less transmitter implementation. Implementation of these structures consists of tunable or fixed delay cells and digital logics to generate narrow pulses. The delay cells have been reduced from eight in [35] for the 5th derivative Gaussian shape to four in [41] for the same order and only six in [33] for the 15th derivative to save power and area.

Despite simple architecture and small in die size, carrier-less transmitters are promising for achieving data rates above 100 Mbps [32], [37], [38]. However, to raise the data rate beyond that, the clock speed, which is the pulse repetition

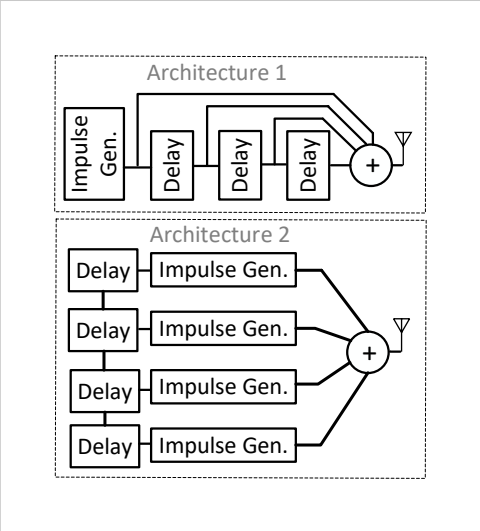

Fig. 5. Typical carrier-less topologies.

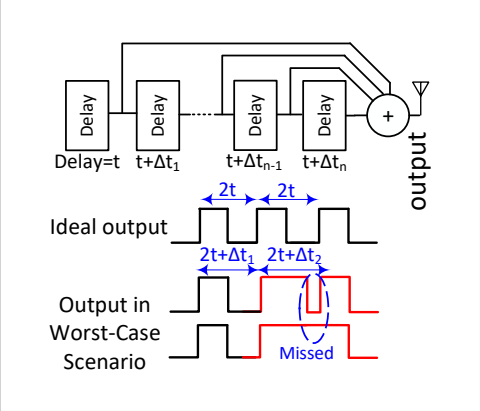

(a)

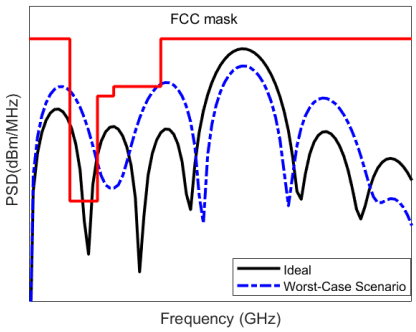

(b)

Fig. 6. Overlapping issue in the edge combining transmitter: ideal and worst-case scenarios. (a) Timing diagram. (b) Corresponding PSD.

frequency (PRF), must be increased, making this structure challenging for further data rate improvements. One of the concerns in edge-combining architectures is the variation of every individual delay cell due to the process, voltage, and temperature (PVT) effect. Significant changes can lead to inconsistent pulse widths and frequency shifting [42]. As presented in Fig. 6 (a), the critical scenario involves the

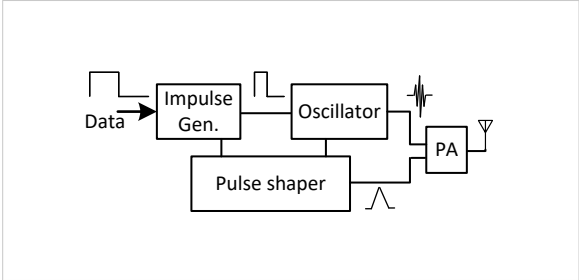

Fig. 7. Typical carrier-based topology.

possibility of a missed pulse in the output. Therefore, the pulse width is doubled which results in a carrier frequency of half. To enhance clarity, a Matlab simulation was conducted, as shown in Fig.6(b). This simulation compares the time domain and frequency spectrum between a typical feedforward edge combining circuit in an ideal setting and the worst-case scenario, where a pulse is missed. According to this figure, uncompensated large delay variations (Δt_n) might result in pulse deformation and spectrum distortion. An overlap-free pulse generation scheme is presented in [43], which utilizes a feedforward compensation technique with interpolators.

B. Carrier-Based Architecture

Carrier-based or up-conversion transmitters have a longer pulse duration, resulting in a narrower bandwidth for ease of implementation. The center frequency of the spectrum is defined by the oscillator's frequency. Fig. 7 shows the diagram of a typical up-conversion IR-UWB transmitter with a triangular pulse envelope. The structure comprises a narrow pulse generator, an oscillator, a pulse shaper to enhance the spectrum, and a power amplifier (PA) at the end of the chain to drive the antenna. The LC-VCO is a good candidate for an oscillator with low phase error [44], [45]; however, it faces some issues. Firstly, the power efficiency of an oscillator during startup is significantly lower than steady-state operation, which can limit the overall efficiency of the transmitter due to the startup time of the oscillator. To overcome the link margin and spectrum compliance, a frequency hopping technique is employed by [46], [47]. Higher VCO frequency in this technique can provide finer frequency resolution and faster-hopping rates, but it may also introduce challenges such as increased power consumption and higher sensitivity to noise and interference. An active inductor is proposed in [48] to save area despite its inherent drawback of higher phase noise. Ring oscillators are employed by [49]–[52] to save power and area, they also have faster ON and OFF switching times. In addition, they have the potential to operate over a broad range of frequencies and can generate multi-phase outputs from the delay cells' output. However, these techniques suffer from frequency instability and poor phase noise, which can hinder high-order modulation implementations for further data rate improvements. This issue is more challenging in the upper-frequency band (e.g., 6-9GHz).

The envelope of the narrow pulse generated by the oscillator can be transformed into various shapes, such as rectangular,

TABLE I
ENVELOPE SHAPES AND THEIR SPECTRAL EFFICIENCIES

Pulse shapes	Gaussian	Half Cosine	Triangular	Rectangular
Spectrum(%) utilization	65	70	68	41
Sidelobe suppression(dBr)	$+\infty$	26.5	30	15.4

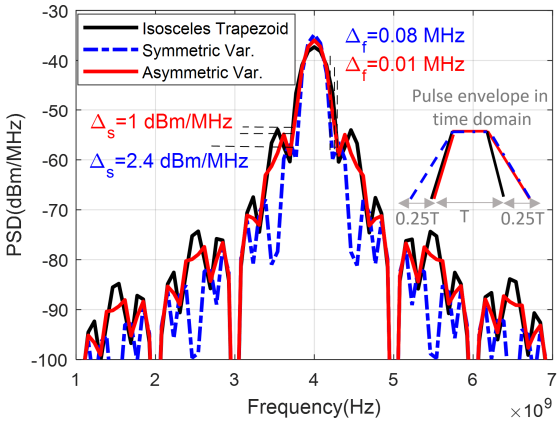

(a)

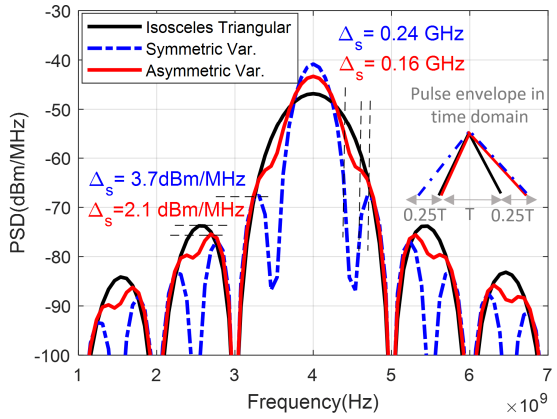

(b)

Fig. 8. Impact of wavelet variations on spectral profile. a) Trapezoidal template, b) Triangular template.

trapezoidal, triangular, Gaussian, etc., to better comply with regulatory standards. TABLE I compares the sidelobe suppression (SLS) performance and in-band spectrum utilization of some of the most common templates [53]. According to this table, a typical rectangular envelope provides almost 16 dBr SLS, which might require extra pulse-shaping to filter the low-frequency components. Other examined templates perform better in SLS, reduce the out-of-band emission, consequently, the need for a dedicated filter is mitigated. Although Gaussian envelope achieves the best SLS, triangular or trapezoidal-based templates are more common due to their easier implementation [42], [54]. In practice, mismatches between NMOS and PMOS devices can lead to deviations in pulse wavelets from ideality. The MATLAB simulations in Fig. 8 study the PSD distortion of trapezoidal and triangular wavelets with

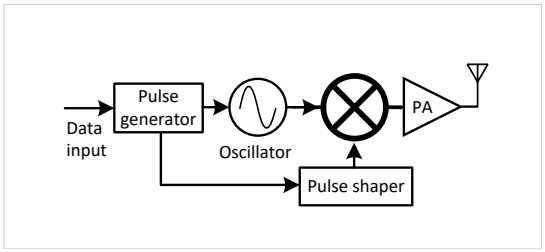

(a)

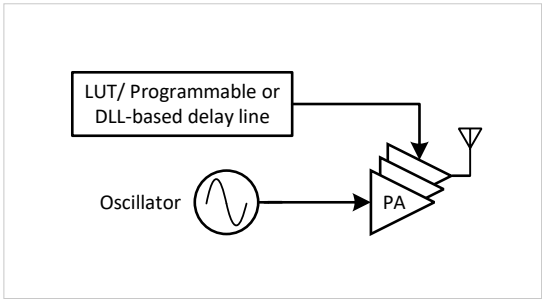

(b)

Fig. 9. Comparison of different pulse shaping techniques, a) Analog approach, b) Digital approach.

symmetric and asymmetric variations. The spectral deviations in the first sidelobe and bandpass frequency of -20 dBm are defined as Δ_s and Δ_f, respectively. The MATLAB simulation results indicate that the output spectrum of a trapezoidal template is less distorted with both types of variations. The envelope nonidealities are systematically analyzed in [55] and an intrinsically symmetrical pulse generator for the isosceles-triangular/trapezoidal envelope is presented. To address the susceptibility to process variations, [42] employs a transistor-sizing-based triangular pulse shaper with a process compensation circuit to achieve -27 dB SLS. The power budget in this technique is only 0.419 mW, which makes it more suitable for low-power applications.

The most common pulse-shaping topologies can be classified into analog and digital structures. In analog approach [56] a low-pass filter (LPF) is employed as the pulse shaper, Fig. 9(a). The shaped pulse is then mixed with a local oscillator (LO) to produce an RF signal. Due to passive elements in the LPF, this technique is area-intensive and poor in tuning once fabricated. Digital pulse shaping techniques have recently gained popularity due to their compatibility with digital processes and duty-cycled operation, which results in reduced power consumption, Fig. 9(b). In this method output voltage should vary linearly with the number of sub-DPAs. However, switching multiple sub-DPA can introduce changes in output impedance, leading to AM-AM distortion [57]. This distortion can adversely affect the pulse, causing an increase in the power of out-of-band sidelobes. Although the linearity can be improved by reducing the output power, this comes at the expense of lower transmission efficiency. To address this issue, a novel AM-AM pre-distortion method is proposed by [53] to improve linearity. Scanning the Look-Up Table (LUT) of the configured delay times might results to more precise AM-AM calibration. [58], [59] propose a power-

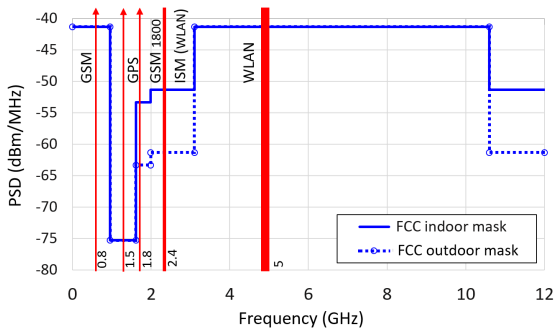

Fig. 10. UWB systems and other existing narrow-band systems [62].

efficient pulse-shaping method that uses a LUT to store pulse amplitude information. This method enables the determination of the pulse template by programming the LUT. This technique suppresses the sidelobe well, however, as the sampling clock depends on the carrier frequency there is a risk of spectrum violation. Another alternative involves using delay-locked loop (DLL) based delay lines to generate the pulse envelope by repeatedly delaying narrow pulses with the same delay step (τ) [60]. This method presents superior sidelobe reduction, however, the pulse template is fixed. A reconfigurable pulse shaper with a high SLS is proposed in [53], which employs a programmable delay line with a calibration method to improve the linearity of the generated pulses. This method also benefits from a nonlinear sampling process to save power compared to the conventional current mode digital power amplifier (DPA), which uses a high-speed digital-to-analog converter (DAC) with a high sampling rate to shape the pulse envelope. Employing programmable delay lines, DPA, and a broadband on-chip matching network with a second harmonic trap, [54] and [53] achieved the highest SLS of better than -30 dB with a power budget of about 3.6mW.

C. Frequency spectrum consideration and interference

The FCC spectral mask for UWB communication sets a maximum isotropic radiated power level of -41.3 dBm/MHz within the bandwidth of 3.1-10.6 GHz. The PSD levels vary for frequencies below 3.1 GHz to avoid interfering with other licensed standards. Meeting the requirements of such a nonuniform mask is demanding. Moreover, Careful consideration of the operating frequency is crucial to maximize in-band power emission without violating mask regulations. Selecting an improper center frequency can impose substantial limitations on the emitted power. For instance, the improper choice of the frequency band, the output PSD is limited by almost 10 dBm/MHz because of mask requirements in [32], [61].

The allocated frequency band of 3.1–10.6 GHz for UWB applications includes multiple narrow-band applications, as shown in Fig. 10. Some researchers [52] believe these adjacent narrow-band channels are not critical due to the localization and near-field nature of IR-UWB transceivers; meanwhile, others are concerned that the coexisted narrow channels can lead to serious interferences in practice. The aspects of interferences to and from UWB systems are studied in [62]. The most common practice to mitigate interference is to adopt the higher UWB band, e.g., 6–9 GHz, at the expense of higher tissue loss [55], [63]. However, some other studies [40], [64]–[66] prefer the crowded lower band of 3–5 GHz due to lower tissue loss, lower central frequency, consequently low power implementation.

To avoid performance degradation due to in-band interferences, multi-sub-band structures are proposed by [40], [64] in the frequency of 3.1-5.1 GHz, while the 5-6 GHz frequency range is avoided to prevent interference from IEEE802.11a (Wi-Fi), which is the major source of interference to UWB systems. Since employing the entire UWB spectrum leads to a better data rate in communications and resolution in positioning systems, covering the entire spectrum with a single UWB pulse is preferred. A fully integrated UWB pulse generator covering the whole BW of 3.1 to 10.6 GHz with several sub-bands is studied at [54], [65]. In [66], a UWB transmitter with 5.5 GHz BW and a tunable notch filter to filter out the frequency of IEEE 802.11a with -30 dB attenuation is presented. However, the complexity and high-power consumption of some of these techniques make them unsuitable for implantable devices, where the area and power budget are restricted.

III. Power Amplifier and Output Stage

The major challenge in UWB power amplifier design is achieving spectral compliance and energy efficiency with limited power and area [67]. Typical PAs working in linear region can achieve spectral compliance but they often suffer from poor power efficiency [68]–[70]. On the other hand, digital and switch mode PAs present better power efficiency [71], while they often require high-order filters or large-area baluns to suppress the radiation in the 0.96-1.61GHz FCC band. Among different DPAs, Class D power amplifiers are more prevalent due to their superior power efficiency [60], [64], [72]. Class-C PAs are also adopted in some designs [45], [73]–[75] with a large inductor in their drain and a tuned LC tank to reduce the distortion of inherently nonlinear amplifiers. A power oscillation is introduced in [44] to maximize energy efficiency, which is connected directly to an on-chip dipole antenna.

The reported FCC infringement in both linear and nonlinear PAs highlights the importance of an efficient filtering stage before the antenna. To suppress the undesired low-frequency components, on-chip baluns with high-pass characteristics can be employed. It is shown that a balun connected in series without capacitors does not fit the FCC mask. Therefore, capacitors are added in series (BCCS) to achieve a three-order high pass filter to satisfy the regulations [64], [76]. An active balun is presented in [77] to drive differential output, save area, and tackle undesired parasitic effects of passive baluns, but spectral compliance is not mentioned in this design. Since this method is bulky, an alternative approach is to suppress the low-frequency components with a capacitively coupled structure [33]. Dual Capacitive coupled (DCC) structures with pre-charged switches [78], [79] are more efficient in SLS reduction than a single capacitor. This method involves

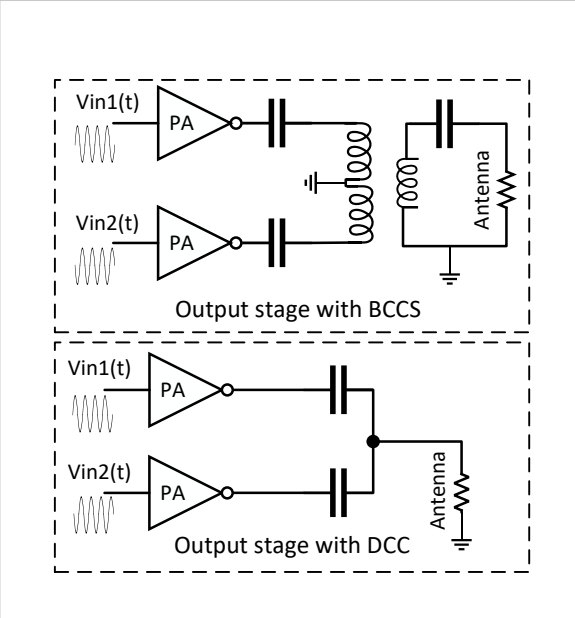

(a)

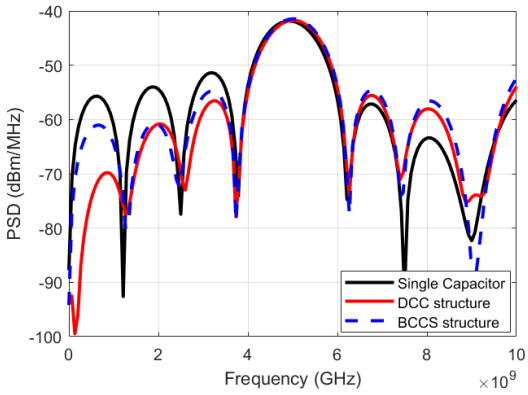

(b)

Fig. 11. Comparison of output filtering stage. a) BCCS and DCC Structures. b) Filtered spectrum.

combining two signals that are in phase at RF but out of phase in their common mode components. The frequency domain circuit analysis shows the spectral effect of the DCC structure. Considering the pulse width asτ_c, the output spectrum of this network in the Laplace domain are given by [79].

$$V_{in1} + V_{in2} = V_{DD}\delta(s) + \frac{V_{DD}}{2}(1 - e^{\frac{-\pi}{\omega_0}s}) \times (1 - e^{-\tau_C s})(\frac{\omega_0^2}{s(s^2 + \omega_0^2)}) \quad (6)$$

At the carrier frequency $(\omega = \omega_0)$, the output signal components remain undisturbed, while at much lower frequencies $(\omega << \omega_0)$, the output is exponentially attenuated regardless of the size of coupling capacitors. In practice, the coupling capacitors should be large to reduce the signal attenuation caused by the deviation of parasitics and coupling capacitors. Besides, they should be identical for better performance. Fig. 11(a) illustrates the structures of BCCS and DCC methods, while Matlab simulations in Fig. 11(b) compares the output spectrum of an ideal transmitter connected to BCCS and DCC filtering stages. To provide a more comprehensive evaluation of these techniques, the spectrum of the transmitter is also presented when connected to a single capacitor used as DC blocking.

The other concern in the output stage is the maximum output amplitude. To set a few examples, the reported output pulses are 140 mV and 44 mV from 1.8 V supply in [37] and [81], respectively. This issue is more serious in the sub-micron CMOS process, in which the supply voltage continuously decreases and driving ability becomes weaker. Increasing the size of MOS devices can enhance the output amplitude, but this comes at the expense of higher power consumption [31]. To mitigate this issue, a pulse booter is proposed in [30] which enhances the gate-source voltage of the MOS device in the output stage by almost two times. The reported output voltage is increased to 96.53 mVp-p from 0.8 V supply. Ensuring output matching is crucial for maximum power transfer from the transmitter to the antenna. In the context of UWB transceivers, achieving a suitable match across a wide operating frequency range presents a particularly challenging task. An off-chip matching network is employed by [82], this method presents certain drawbacks such as increased area, cost, and signal loss in passive elements and the signal path. Achieving broadband matching typically necessitates the use of multiple bulky inductors and capacitors, as demonstrated in [83], [84]. A fully integrated single transformer is presented by [53] for low-area output matching. In [55], a current-reused common drain and common source combined amplifier was introduced. This innovative design possesses an inherent wide-band output matching characteristic, effectively reducing the reliance on high-order LC matching and bulky passive baluns. To address the constraints imposed by neurosurgical requirements, it is imperative to co-design both the antenna and the UWB transmitter in a manner that fulfills the desired objectives including the compact size and the ability to support the UWB operating band [63], [85]. The development and evaluation of flexible UWB antennas for implants is studied in [86].

TABLE II provides a comprehensive summary of the performance characteristics exhibited by various transmitter architectures. In terms of PSD and output swings, the edge-combining techniques generally demonstrate lower values compared to up-conversion transmitters. However, it is worth noting that edge-combining techniques consume lower energy per bit, which translates to their higher energy efficiency. Among the architectures considered, the transmitter presented in [80] stands out with the largest output swing. This achievement is attributed to the implementation of a tuned LC tank that resonates in a steady state during transmission and a class-C power amplifier. However, it is important to acknowledge that this architecture comes at the expense of occupying the largest active area.

IV. IR-UWB RECEIVERS

In unidirectional implants, the receiver of an IR-UWB radio can be implemented externally with relaxed features in terms

TABLE II
PERFORMANCE COMPARISON OF IR-UWB TRANSMITTERS

Process (nm)	Architecture	Mod.	BW (GHz)	Data rate (Mbps)	PSD (dBm/MHz)	Vp-p (mV)	Power (mW)	Energy (pJ/b)	Area (mm2)	App.	Ref
180	Edge-combination (15th deriv.), DPA, single Cap.	OOK	3.1-10.6	31.25	-50*	56	NA	12.5	0.02	Multi purpose	[33]
180	Edge-combination (5th driv.), pulse booster, DPA, single Cap.	OOK	Sub-GHz	50	-65*	96.53	0.559	11.18	0.0067	Bio.	[30]
65	Edge-combination (15th deriv.), DPA, DCC, pre-charging switch	S-OOK	3.1-8	10	-55*	750	0.216	21.6	0.03	Bio.	[78]
180	Edge-combination (6th deriv.), Linear PA, combined filter	BPSK-PAM	3.5-7	715	-41.3	1000	21.6	30	0.22	IoT	[68]
65	Edge-combination (deriv. NA), DPA, filter	OOK	3-10.6	200	-50*	200	0.86	4.3	0.065	Bio.	[43]
28 FDSOI	Carrier-based, digital pulse-shaping filter combined with DPA	BPM	NA	27.24	-55	350	0.38	14	0.095	IoT	[59]
28	Carrier-based, pulse shaping DPA (triangular), DPA, DCC	BPSK	3-10	27.24	-41*	200*	4.9	180	0.154	Ranging	[60]
130	Carrier-based, tuned LC tanks, Class C-PA, filter	OOK	3-5	230	-41*	1600	3.7	21	1.19	Bio.	[80]

*Estimated from reported simulation results

of power and design. Some bidirectional UWB transceivers employ IR-UWB for high-density data transmission (up-link) and a narrow-band link as a receiver (down-link) for low data rate control messages [37], [38]. This innovative approach allows the Tx and Rx to use the same antenna and communicate concurrently in different frequency bands. However, IR-UWB receivers offer several advantages over their narrow-band counterparts. The impulsive nature of pulses employed in UWB radios provides improved accuracy, better immunity against interference, and robustness to multi-path fading [87]–[89]. This section introduces the conventional UWB receivers and discusses the considerations for mitigating narrow-band interference in receiver design.

A. Receiver architectures

Conventional UWB receivers can be classified into two methodologies, coherent and non-coherent. Coherent receivers require accurate timing and synchronization, which poses challenges in receiving short-duration pulses. Thus, low jitter and accurate delay blocks are necessary for demodulation. Besides, these receivers should be able to handle multi-path copies of the transmitted pulses effectively. In essence, coherent architectures with high power consumption suit better for localization applications with higher accuracy, longer communication range, and superior robustness requirements [20], [58], [89]–[91]. Fig. 12(a) depicts the block diagram of a typical coherent receiver with an energy detection mechanism.

The non-coherent architecture offers a low-power solution that avoids the need for sophisticated channel estimation. These advantages make non-coherent receivers more preferred for biomedical implants over their coherent counterpart even though they come at the expense of degraded sensitivity and poor bit error rate (BER). The non-coherent receiver scheme varies considerably from design to design. For example, some studies mix the incoming signal with a local oscillator, then the energy of the received signal is measured from generated I and Q components. The use of passive mixers can be attractive from a power dissipation perspective [92], while an active mixer introduces conversion gain and relaxes the requirements on the front-end amplifiers. Other methods, such as the energy detector (ED) methodology [46], [93] utilize an LNA followed by a variable gain amplifier to match the input and provide significant gain for the following blocks. The amplified signal is then applied to the ED, which consists of a down-converting squarer and a windowed integrator, followed by a comparator as a decision block, Fig. 12(b). ED structures might be preferred because of their low complexity, but a large amplification is required to detect poor signals. Achieving high amplification gain (>40 dB) with large bandwidth is

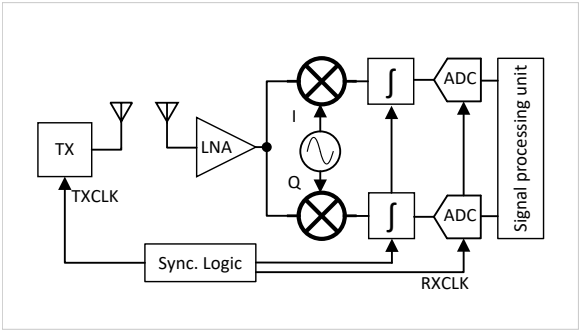

(a)

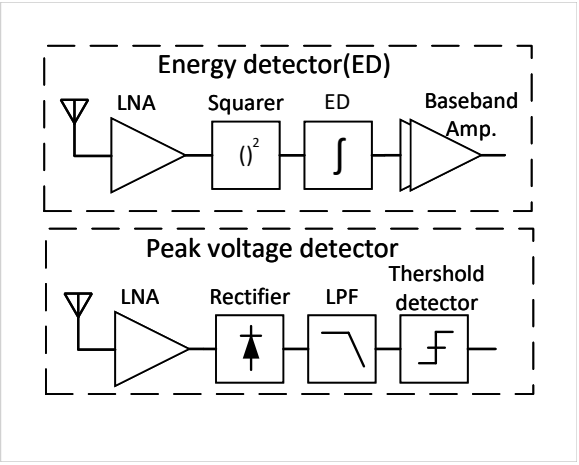

(b)

Fig. 12. Typical receiver architectures. a) Coherent architecture, b) Non-coherent architecture.

inefficient in low-power CMOS applications. A peak voltage detection (PD) technique is presented in [94], which relaxes design requirements regarding the gain stages and addresses the concerns for many short-range communications. The key element of this design is the rectifier implemented by a chain of inverters to improve sensitivity, Fig. 12(b).

TABLE III evaluates some of the state-of-art-IR-UWB receivers. According to this table, coherent receivers achieved sensitivity better than -102 dBm at the expense of several times higher DC power. Regarding non-coherent receivers, ED structures achieved higher data rates, while PD architecture presents better sensitivity.

B. Narrow-band Interferes (NBI)

Given the UWB nature of the transmitted signal, the receiver front end should operate over a very large bandwidth, making them vulnerable to interference. Besides, the introduction of wireless standards like Wi-Fi 6, 5G, etc., NBI immunity becomes increasingly critical for UWB transceivers. NBI considerations can be relaxed in short-range radios, however, as the trend is towards increasing communication range, special measures should be taken to tolerate interference. Filtering and excluding occupied frequency bands can mitigate NBI, but it is not always sufficient, especially in a longer communication range. The other technique is bandpass filtering in the baseband. Since bandwidth of UWB signals is a few ten times wider than the NBIs, the energy of NBI is down-converted to lower frequencies, while the UWB signals are transferred to much higher baseband frequencies. Typical ED receivers employ integrators and amplifiers in the baseband with larger gain at DC, which further degrades NBI robustness. To reject NBIs while only losing a small fraction of the UWB signal, a subsequent LPF and HPF after the mixer are suggested by [98], as illustrated in Fig. 13. The cut-off frequency of LPF is set to almost half of the UWB signal and the cut-off frequency of HPF is set as almost twice of NBI signal BW (IEEE 802.11 a/b/g for instance). This method rejects the NBI with 2 MHz and 20 MHz BW by 26 dB and 7.6 dB, respectively.

V. IMPROVEMENTS AND FUTURE PERSPECTIVES

The IR-UWB radios with their unique features have received great attention from various applications, including ranging, communication, or both. Several application-oriented improvements have been reported to enhance the data rate, communication distance, power efficiency, and system reliability. However, as this review paper focuses on brain implants, improvements around this dedicated application are discussed.

One of the recent trends in neural recording implants involves distributing multiple high-density micro-electrode arrays (MEAs) across different brain regions. Given the typical sensing channel sample rate of 20-50KSps and an ADC with 10-bit resolution, the required data transfer rate for multiple MEAs with over 1000 recording channels would be in the range of Gbps [63]. Although data reduction techniques can alleviate the bandwidth requirements for the given data transmission, transferring raw data from an implant is preferred for optimization and diagnosis purposes. The major challenge in enhancing the data rate is the limited power budget. Moreover, low on-chip power density is required to avoid tissue heating. The other challenge is the strictly limited communication range, typically in the centimeter range. In IR-UWB radio, the transmitted power (P_{TX}) and SNR at the input of the receiver (SNR_{Rx}) are defined as [95].

$$P_{TX} = PRF \times E_p \tag{7}$$

$$SNR_{Rx} = E_p \times \frac{Path_{LOSS}}{Noise} \tag{8}$$

Here, E_P and $Path_{Loss}$ indicate the energy of the transmitted pulse and the path loss, respectively. So, communication distance is defined by E_P and it should be increased to improve the link margin. However, the maximum allowed $P_{TX}$is limited by the FCC [95].

$$P_{TX} - 41.3\frac{dBm}{MHz} + 10 \times log(BW) \tag{9}$$

Therefore, there is a trade-off between communication distance and high data rate. In other words, sacrificing the data rate proportional to pulse repetition frequency (PRF) can enhance the link margin. However, this issue can be mitigated by reducing the data-rate dependence on the symbol period for high-efficient communication. Pulse width modulation (PWM) can relax this dependence, but the pulse-width modulation with an analog approach restricts the modulation speed, limiting the communication speed to below 100 Mb/s. To mitigate this issue, digitalized multi-PPM (D-MPPM) is employed by [95] to achieve the data rate of 500Mbps. D-MPPM modulates input data by two pulses ($Data_{x,y}$ pulse) among n different valid positions at specified time steps (T_{step}) with respect to the sync pulse. This modulation scheme can be implemented using low-power digital circuits such as digital-to-time (DTC) or time-to-digital converters (TDC) for modulation and demodulation. To further improve the data throughput to the Gbps level, the extended version of D-MPPM, called E-MPPM is introduced in [99], [100] with a modulation order of 3 to enhance the data rate to 1.125 Gbps with the radio range of 2 m. The E-MPPM modulates input data into a time difference (TD) utilizing sync and data pulses to increase modulation efficiency. TABLE IV Compares the performance of OOK, D-MPM, and E-MPPM modulations [99]. In this table, M refers to the number of digital bits that can be modulated in one symbol period, and is defined as $log_2(n(n+1)/2)$ and the data rate is $M \times SybmolPriod[bps]$. It is also worth noting that sync pulses in the E-MPPM scheme restrict the modulation order by one-third.

To overcome this limitation, [101] improves the modulation order to 7 with a 3D hybrid impulse modulation composed of 4PAM-8PSK-4PPM and achieves the data rate of 1.66Gbps. This work employs an injection-locked negative skewing ring-based digital-control oscillator for a faster transition and better phase noise performance. In this method, the operating frequency is improved by almost 30% compared to traditional delay cells. However, 8PSK modulation demands a high-speed 8-phase carrier and a power-costly up-conversion design. Moreover, the transmission range is decreased since the output pulse amplitude is reduced due to PAM modulation.

TABLE III
PERFORMANCE COMPARISON OF IR-UWB RECEIVERS

Process (nm)	Modulation	BW (GHz)	Data rate (Mbps)	Power (mW)	Sensitivity (dBm)	Distance (m)	Energy (pJ/b)	Application	Method	Ref
28	BPM-BPSK	3-10	27.2	22.6	-83	NA	830	Ranging	Coherent	[90]
40	BPM-BPSK	6.5-10	31.2	150	-102	NA	480	WSN	Coherent	[58]
130	DB-BPSK, OOK	3-5	100	30.5	-85.8	1.9	305	WBAN/Biomedical	Noncoherent (PD)	[94]
65	OOK	7.25-9.5	500	13.3	-59	1.2	26.6	Biomedical	Noncoherent (ED)	[46]
65	D-MPPM	3-5	500	34.7	-61	1	69.4	IoT/Biomedical	Noncoherent (ED)	[95]
130	OOK/FSK	2.8-5	150	13.2	-72	NA	88	IoT	Noncoherent (ED)	[93]
130	RA-OOK	3-5	100	14.4	-89.3	2.36	144	WBAN/Biomedical	Noncoherent (ED)	[96]
180	OOK	3.4-4.5	200	15.56	-54	NA	78	Biomedical	Noncoherent (ED)	[97]

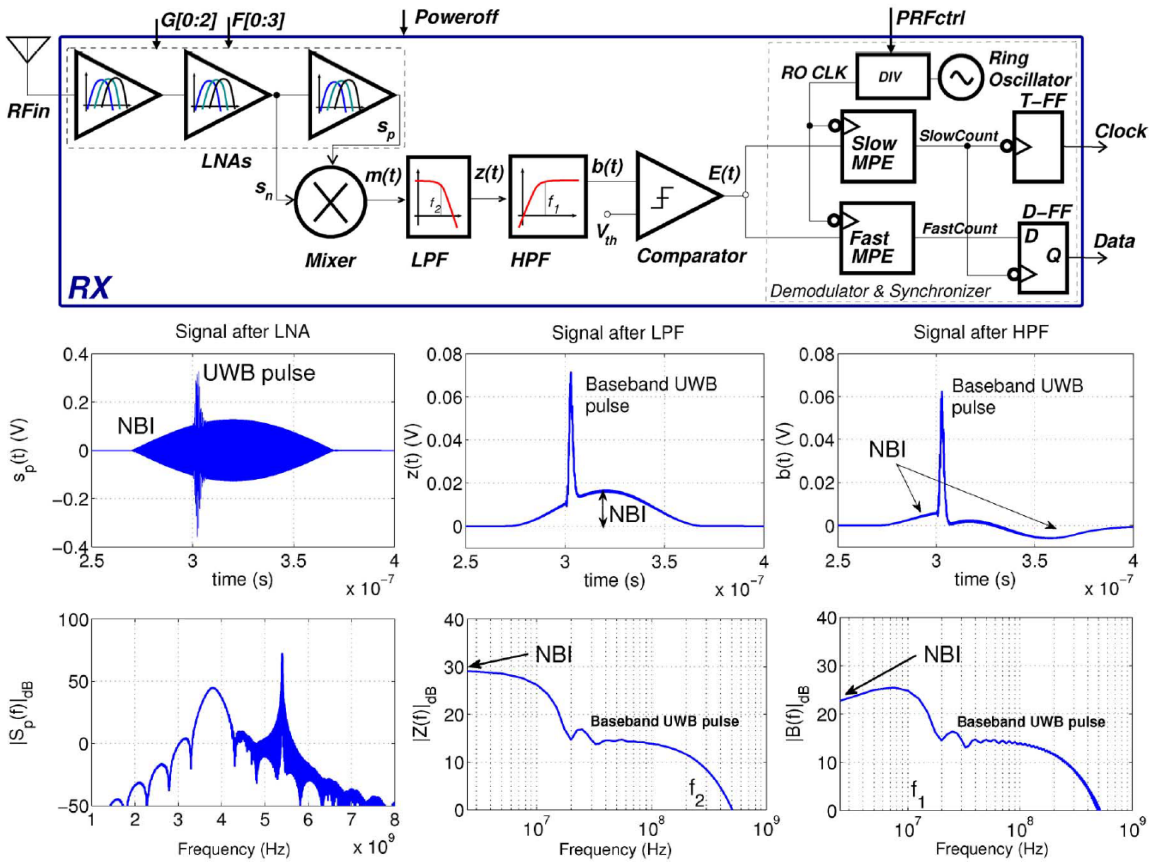

Fig. 13. NBI-tolerate coherent ED receiver for UWB signals with the frequency and time domain presentation of the NBI reduction mechanism [98].

TABLE IV
PERFORMANCE COMPARISON

	OOK	D-MPPM	E-MPPM
Number of pulses per symbol period	0.5	2	3
n	1	32	32
M	1	5	9
Symbol period [a]	τ_{Dura}	$2 \times \tau_{Dura}$ $+(n-1) \times \tau_{step}$	$3 \times \tau_{Dura}$ $+(n-1) \times \tau_{step}$
Duty gain (G_{duty})[b]	2	1.4	1.27
Data rate gain (G_{DR})[c]	1	1.79	2.37
Required E_b/N_0 [dB]	12.5	17.6	17.9
FoM[d]	2	2.5	3

[a] Symbol period = $N_{pulse} \times \tau_{Dura} + (n-1) \times \tau_{step}$
[b] Duty gain (G_{duty}) = Symbol period / ($N_{pulse} \times \tau_{Dura}$)
[c] Data rate gain (G_{DR}) = $M \times \tau_{Dura}$/Symbol period
[d] FoM = $G_{duty} \times G_{DR} = M/N_{pulse}$

All digital designs with edge-combing techniques can be employed to achieve higher data rates with better power efficiency. A hybrid-modulation carrier-less transmitter is proposed in [102], combining the Differential 16-Pulse-Position-Modulation (D16PPM), PWM, and differential binary phase-shift keying (DBPSK) to achieve a modulation order of 6. TABLE V summarizes the performances of state-of-art architectures with a data rate in the Gbps range. All references studied in this table, excluding [99], [100], avoid the frequency band of 5 GHz which contains the most powerful interference of Wi-Fi and 5G. According to this table, all-digital designs, besides improved modulation techniques, achieved the best performance in comparison to the other state-of-the-art works. The IR-UWB has the potential for further improvements and more investigations are still required to bring this technology to maturity. Since the current trends focus on transceiver

TABLE V
STATE-OF-THE-ART POWER EFFICIENT AND HIGH DATA RATE IR-UWB DESIGNS

Ref	[103]	[99][100]	[63][101]	[102]	
Process(nm)	130	65	28	40	
Frequency band (GHz)	3.5-4.5	3.5-6	6-9	3.1-5	
Architecture	Edge	Edge	Up-conversion	Edge	
modulation	OOK	E-MPPM	4PPM+8PSK +4PAM	D16PPM+ PWM+DBPSK	
Mod. order	2-bit	3-bit	7-bit	6-bit	
Data rate (Gbps)	1	1.125	1.66	1.8	
Power (mW)	5(Tx)	9.7(Tx) 28(TRx)	9.69(Tx)	4.09(Tx)	
Tx Energy efficiency [pJ/bit]	5	8.2	5.8	2.3	
Max. Vp-p(mV)	50	200	120	140	
Tissue type	NA	No tissue	15mm Skin/fat	18mm Skin/fat	
Sensitivity (dBm)	-	-68	-	-	
BER	NA	$<10^{-3}$	10^{-4}	10^{-3}	10^{-4}
Radio range (m)	NA	2	0.02	0.2	0.15
Application	Multi purpose & BMI	Multi purpose	Neural recording	Neural recording	

designs with higher data rates and longer communication distances, future investigations should concern efficient techniques to improve NBI immunity, enhanced sensitivity, and better BER with restricted DC power.

The typical reported sensitivity and the BER are in the range of -60 dBm and 10^{-3}, respectively. To improve the sensitivity with good NBIs and low power, an uncertain intermediate frequency (IF) with a pulse-triggered ED receiver is presented in [104] with a sensitivity of -77 dBm. In this design, the required quality factor (Q) for filters is relaxed, contrary to narrow-band uncertain-IF wake-up receivers [105], [106]. Furthermore, the S-OOK modulation mitigates the synchronization issue in the baseband. TABLE VI evaluates this architecture with other traditional receiver architectures. The uncertain-IF architecture, with an additional BPF and an extra gain stage before squarer at the IF stage provides better NBI tolerance and sensitivity than the traditional non-coherent UWB receivers. For further improvements, high-frequency PLL is replaced with a calibrated open-loop DCO and a fast start-up oscillator (few ns) to significantly reduce power. This structure is further improved in [107], to achieve the sensitivity of -81 dBm for the data rate of 10 Mbps and the energy of 380 and 540 pJ/b for the transmitter and receiver, respectively. The data rate in both studied manuscripts is restricted by the demodulation processing delay, which is dictated by ranging applications and might be relaxed in others with lower resolution requirements. Despite its enhanced sensitivity, low energy efficiency poses a significant challenge for BMIs.

Artificial Intelligence has recently been used to improve the reliability of RF communication systems [108]–[110]. AI-assisted signal processing can filter out the clutter and harmonics in demodulated signals, allowing targeted information to be extracted from the received signal with a modified filter instead of typical filters with complicated tuning parameters. Moreover, AI algorithms can improve IR-UWB circuit design

TABLE VI
UNCERTAIN-IF UWB RX VS TRADITIONAL ARCHITECTURES

	Noncoherent	Coherent	Uncertain IF
NBI tolerate	Weak	Strong	Good
Sensitivity	Weak	High	Good
Power	Low	High	Moderate
Design complex	Low	High	Moderate
Intermittent operation	Yes	No	Yes

optimization by predicting performance and identifying the optimal configuration. Machine learning can improve IR-UWB transceivers in biomedical implants by optimizing their design, enhancing their signal processing capabilities, and optimizing their power consumption [111], [112]. As machine learning continues to advance, it is expected that AI plays an increasingly important role in the development of biomedical implants and other wireless communication systems.

Powering BMIs remains a critical challenge that hinders improvements in data rate, communication range, and implant lifetime. Integration with power-harvesting front ends is also among future challenges. The idea of employing LC tanks instead of a typical oscillator was initially presented in [113] and then improved in [80]. In a steady state, the employed LC tank eliminates the need for periodically turning on and off the oscillator. Therefore, the startup time of the oscillator no longer limits the bit rate, and power efficiency is further enhanced with the proposed clipped-sinusoid pulse generation scheme. An additional advantage is that the transmitter can simultaneously transmit data and be inductively powered. This technique achieves a BER of 10^{-6} over the communication distance of 2 m.

VI. CONCLUSION

IR-UWB transceivers show great potential for improving the functionality and performance of multi-channel BMIs. The primary challenges faced by multi-channel BMIs are the stringent requirements for high data rates and ultra-low power consumption. The IR-UWB transceivers, with high energy efficiency, flexible data rate, and simple architecture, have emerged as a promising technology for brain implants. In this overview article, we have analyzed various implementation techniques for IR-UWB transceivers to identify the bottleneck of each architecture. An in-depth study on high data throughput transceivers concludes that all-digital design methodologies are more appropriate for ultra-low power applications, while hybrid modulation techniques combining various modulation schemes can achieve data rates exceeding Gbps. Most reports are based on biological-equivalent phantoms or simulation models, and experimental evolution with living bodies or noisy environments has rarely studied enforcing future works to consider practical issues. We believe that compatibility with energy harvesting designs and extending communication distance with a restricted power budget define the future challenges for IR-UWB transceivers for neural recording implants. Additionally, AI-assisted techniques can further enhance the performance of IR-UWB transceivers by

optimizing their design, signal processing capabilities, and power consumption.

ACKNOWLEDGMENTS

The authors would like to acknowledge funding support from Westlake University, grant number 10318A992001; Leading Innovative and Entrepreneur Team Introduction Program of Zhejiang, grant number 2020R01005; and Zhejiang Key R&D Program No. 2021C03002.

REFERENCES

[1] I. H. Stevenson and K. P. Kording, "How advances in neural recording affect data analysis," *Nature neuroscience*, vol. 14, no. 2, pp. 139–142, 2011.

[2] Z. S. Chen and B. Pesaran, "Improving scalability in systems neuroscience," *Neuron*, vol. 109, no. 11, pp. 1776–1790, 2021.

[3] M. A. Ibrahim and M. Onabajo, "A 0.061 nj/b 10 mbps hybrid bf-psk receiver for internet of things applications," *IEEE Transactions on Circuits and Systems I: Regular Papers*, vol. 69, no. 5, pp. 1919–1931, 2022.

[4] A. Nikoofard, H. A. Zadeh, and P. P. Mercier, "A 0.6-mw 16-fsk receiver achieving a sensitivity of- 103 dbm at 100 kb/s," *IEEE Journal of Solid-State Circuits*, vol. 56, no. 4, pp. 1299–1309, 2021.

[5] K.-W. Cheng and S.-E. Chen, "An ultralow-power ook/bfsk/dbpsk wake-up receiver based on injection-locked oscillator," *IEEE Transactions on Very Large Scale Integration (VLSI) Systems*, vol. 29, no. 7, pp. 1379–1391, 2021.

[6] S.-Y. Lee, P.-H. Cheng, C.-F. Tsou, C.-C. Lin, and G.-S. Shieh, "A 2.4 ghz ism band ook transceiver with high energy efficiency for biomedical implantable applications," *IEEE transactions on biomedical circuits and systems*, vol. 14, no. 1, pp. 113–124, 2019.

[7] M. Zgaren, A. Moradi, L.-F. Tanguay, and M. Sawan, "Ism-band 902-to 928-mhz fsk transceiver with scalable performance for medical devices," *International Journal of Circuit Theory and Applications*, vol. 46, no. 12, pp. 2266–2282, 2018.

[8] M. Ali, H. Shawkey, A. Zekry, and M. Sawan, "One mbps 1 nj/b 3.5–4 ghz fully integrated fm-uwb transmitter for wban applications," *IEEE Transactions on Circuits and Systems I: Regular Papers*, vol. 65, no. 6, pp. 2005–2014, 2017.

[9] J. Chen, M. Tarkhan, H. Wu, F. H. Noshahr, J. Yang, and M. Sawan, "Recent trends and future prospects of neural recording circuits and systems: A tutorial brief," *IEEE Transactions on Circuits and Systems II: Express Briefs*, vol. 69, no. 6, pp. 2654–2660, 2022.

[10] M. Sawan, J. Yang, M. Tarkhan, J. Chen, M. Wang, C. Wang, F. Xia, Y.-H. Chen *et al.*, "Emerging trends of biomedical circuits and systems," *Foundations and Trends® in Integrated Circuits and Systems*, vol. 1, no. 4, pp. 217–411, 2021.

[11] B. Wang, H. Song, W. Rhee, and Z. Wang, "Overview of ultra-wideband transceivers—system architectures and applications," *Tsinghua Science and Technology*, vol. 27, no. 3, pp. 481–494, 2021.

[12] T. Terada, R. Fujiwara, G. Ono, T. Norimatsu, T. Nakagawa, M. Miyazaki, K. Suzuki, K. Yano, A. Maeki, Y. Ogata *et al.*, "Intermittent operation control scheme for reducing power consumption of uwb-ir receiver," *IEEE journal of solid-state circuits*, vol. 44, no. 10, pp. 2702–2710, 2009.

[13] K. Y. Yazdandoost and R. Miura, "Sar studies for uwb implanted antenna for brain-machine-interface application," in *2016 10th European Conference on Antennas and Propagation (EuCAP)*. IEEE, 2016, pp. 1–4.

[14] K. M. Thotahewa, J.-M. Redouté, and M. R. Yuce, "Sar, sa, and temperature variation in the human head caused by ir-uwb implants operating at 4 ghz," *IEEE transactions on microwave theory and techniques*, vol. 61, no. 5, pp. 2161–2169, 2013.

[15] K. M. Thotahewa, J.-M. Redoutè, and M. R. Yuce, "Propagation, power absorption, and temperature analysis of uwb wireless capsule endoscopy devices operating in the human body," *IEEE Transactions on Microwave Theory and Techniques*, vol. 63, no. 11, pp. 3823–3833, 2015.

[16] F. Khan, S. Azou, R. Youssef, P. Morel, E. Radoi, and O. A. Dobre, "An ir-uwb multi-sensor approach for collision avoidance in indoor environments," *IEEE Transactions on Instrumentation and Measurement*, vol. 71, pp. 1–13, 2022.

[17] H.-B. Li, K. Takizawa, T. Kagawa, F. Kojima, and R. Miura, "Improvement on localization accuracy of ir-uwb by adapting time bias inner transceiver," in *2019 International Conference on Computing, Networking and Communications (ICNC)*. IEEE, 2019, pp. 116–120.

[18] R. W. C. Ling, A. Gupta, A. Vashistha, M. Sharma, and C. L. Law, "High precision uwb-ir indoor positioning system for iot applications," in *2018 IEEE 4th World Forum on Internet of Things (WF-IoT)*. IEEE, 2018, pp. 135–139.

[19] D. Li, X. Wang, D. Chen, Q. Zhang, and Y. Yang, "A precise ultra-wideband ranging method using pre-corrected strategy and particle swarm optimization algorithm," *Measurement*, vol. 194, p. 110966, 2022.

[20] D. Morche, G. Masson, S. De Rivaz, F. Dehmas, S. Paquelet, A. Bisiaux, O. Fourquin, J. Gaubert, and S. Bourdel, "Double-quadrature uwb receiver for wide-range localization applications with sub-cm ranging precision," *IEEE Journal of Solid-State Circuits*, vol. 48, no. 10, pp. 2351–2362, 2013.

[21] D. Anzai, K. Katsu, R. Chavez-Santiago, Q. Wang, D. Plettemeier, J. Wang, and I. Balasingham, "Experimental evaluation of implant uwb-ir transmission with living animal for body area networks," *IEEE Transactions on Microwave Theory and Techniques*, vol. 62, no. 1, pp. 183–192, 2013.

[22] S. Perez-Simbor, C. Andreu, C. Garcia-Pardo, M. Frasson, and N. Cardona, "Uwb path loss models for ingestible devices," *IEEE Transactions on Antennas and Propagation*, vol. 67, no. 8, pp. 5025–5034, 2019.

[23] H. Bahrami, S. A. Mirbozorgi, L. A. Rusch, and B. Gosselin, "Biological channel modeling and implantable uwb antenna design for neural recording systems," *IEEE Transactions on Biomedical Engineering*, vol. 62, no. 1, pp. 88–98, 2014.

[24] R. Hazra and A. Tyagi, "A survey on various coherent and non-coherent ir-uwb receivers," *Wireless Personal Communications*, vol. 79, pp. 2339–2369, 2014.

[25] J. A. Zhang, "8.2 uwb basics," *Advances in Broadband Communication and Networks*, 2022.

[26] Y. Andreyev, "Analytical model of an energy detector for ultra-wideband chaotic communications," *Electronics*, vol. 12, no. 4, p. 954, 2023.

[27] S. Nagaraj and F. G. Rassam, "Improved noncoherent uwb receiver for implantable biomedical devices," *IEEE Transactions on Biomedical Engineering*, vol. 63, no. 10, pp. 2220–2225, 2015.

[28] M. Crepaldi, G. N. Angotzi, and L. Berdondini, "A 0.34 mm 2 1 gb/s non-coherent uwb receiver architecture with pulse enhancement and double pll clock/data packet recovery," *IEEE Transactions on Circuits and Systems I: Regular Papers*, vol. 66, no. 7, pp. 2735–2748, 2019.

[29] X. Zhang, Z. Zhang, Y. Li, C. Liu, Y. X. Guo, and Y. Lian, "A 2.89μw dry-electrode enabled clockless wireless ecg soc for wearable applications," *IEEE journal of solid-state circuits*, vol. 51, no. 10, pp. 2287–2298, 2016.

[30] X. Tong, D. An, and J. Li, "Area-and energy-efficient sub-ghz impulse radio uwb transmitter with output amplitude enhancement for biomedical implants," *IEEE Transactions on Circuits and Systems II: Express Briefs*, vol. 68, no. 6, pp. 1807–1811, 2020.

[31] L. Wang, C.-H. Heng, and Y. Lian, "A sub-ghz mostly digital impulse radio uwb transceiver for wireless body sensor networks," *IEEE Journal on Emerging and Selected Topics in Circuits and Systems*, vol. 4, no. 3, pp. 344–353, 2014.

[32] J. Radic, M. Brkic, A. Djugova, M. Videnovic-Misic, B. Goll, and H. Zimmermann, "Ultra-low power low-complexity 3–7.5 ghz ir-uwb transmitter with spectrum tunability," *IET circuits, devices & systems*, vol. 14, no. 4, pp. 521–527, 2020.

[33] B. Wei, T. Chen, C. Lu, W. Xu, Y. Zhang, X. Wei, H. Yue, and J. Duan, "An all-digital frequency tunable ir-uwb transmitter with an approximate 15th derivative gaussian pulse generator," *Integration*, vol. 69, pp. 301–308, 2019.

[34] H. Sheng, P. Orlik, A. M. Haimovich, L. J. Cimini, and J. Zhang, "On the spectral and power requirements for ultra-wideband transmission," in *IEEE International Conference on Communications, 2003. ICC'03.*, vol. 1. IEEE, 2003, pp. 738–742.

[35] H. Kim and Y. Joo, "Fifth-derivative gaussian pulse generator for uwb system," in *2005 IEEE Radio Frequency integrated Circuits (RFIC) Symposium-Digest of Papers*. IEEE, 2005, pp. 671–674.

[36] H. Kassiri, A. Bagheri, N. Soltani, K. Abdelhalim, H. M. Jafari, M. T. Salam, J. L. P. Velazquez, and R. Genov, "Battery-less tri-band-radio neuro-monitor and responsive neurostimulator for diagnostics and treatment of neurological disorders," *IEEE Journal of Solid-State Circuits*, vol. 51, no. 5, pp. 1274–1289, 2016.

[37] S. A. Mirbozorgi, H. Bahrami, M. Sawan, L. A. Rusch, and B. Gosselin, "A single-chip full-duplex high speed transceiver for multi-site stimulating and recording neural implants," *IEEE transactions on biomedical circuits and systems*, vol. 10, no. 3, pp. 643–653, 2015.

[38] M. Rezaei and B. Gosselin, "Low-power high-speed wireless transceivers and antennas for large-scale neural implants," in *2016 14th IEEE International New Circuits and Systems Conference (NEWCAS)*. IEEE, 2016, pp. 1–4.

[39] A. Apsel, X. Wang, and R. Dokania, *Design of ultra-low power impulse radios*. Springer Science & Business Media, 2013, vol. 124.

[40] A. T. Phan, J. Lee, V. Krizhanovskii, Q. Le, S.-K. Han, and S.-G. Lee, "Energy-efficient low-complexity cmos pulse generator for multiband uwb impulse radio," *IEEE Transactions on Circuits and Systems I: Regular Papers*, vol. 55, no. 11, pp. 3552–3563, 2008.

[41] X. Wang, S. Fan, H. Tang, L. Lin, J. Liu, Q. Fang, H. Zhao, A. Wang, L.-w. Yang, and B. Zhao, "A whole-chip esd-protected 0.14-pj/p-mv 3.1–10.6-ghz impulse-radio uwb transmitter in 0.18-μm cmos," *IEEE transactions on microwave theory and techniques*, vol. 59, no. 4, pp. 1109–1116, 2011.

[42] H. U. Mahmood, D. R. Utomo, J. Kim, and S.-G. Lee, "A 27 db sidelobe suppression, 1.12 ghz bw- 10db uwb pulse generator with process compensation," *IEEE Transactions on Circuits and Systems II: Express Briefs*, vol. 68, no. 8, pp. 2805–2809, 2021.

[43] Y.-J. Lin, S.-Y. Park, X. Chen, D. Wentzloff, and E. Yoon, "4.32-pj/b, overlap-free, feedforward edge-combiner-based ultra-wideband transmitter for high-channel-count neural recording," *IEEE Microwave and Wireless Components Letters*, vol. 28, no. 1, pp. 52–54, 2017.

[44] H. Rahmani and A. Babakhani, "A wirelessly powered reconfigurable fdd radio with on-chip antennas for multi-site neural interfaces," *IEEE Journal of Solid-State Circuits*, vol. 56, no. 10, pp. 3177–3190, 2021.

[45] D. K. Biswas and I. Mahbub, "A low-power duty-cycled impulse-radio ultrawideband (ir-uwb) transmitter with bandwidth and frequency reconfigurability scheme designed in 180 nm cmos process," in *2021 IEEE radio and wireless symposium (RWS)*. IEEE, 2021, pp. 49–52.

[46] S. Geng, D. Liu, Y. Li, H. Zhuo, W. Rhee, and Z. Wang, "A 13.3 mw 500 mb/s ir-uwb transceiver with link margin enhancement technique for meter-range communications," *IEEE Journal of Solid-State Circuits*, vol. 50, no. 3, pp. 669–678, 2015.

[47] F. Chen, Y. Li, D. Liu, W. Rhee, J. Kim, D. Kim, and Z. Wang, "9.3 a 1mw 1mb/s 7.75-to-8.25 ghz chirp-uwb transceiver with low peak-power transmission and fast synchronization capability," in *2014 IEEE International Solid-State Circuits Conference Digest of Technical Papers (ISSCC)*. IEEE, 2014, pp. 162–163.

[48] K. Ture, A. Devos, F. Maloberti, and C. Dehollain, "Area and power efficient ultra-wideband transmitter based on active inductor," *IEEE Transactions on Circuits and Systems II: Express Briefs*, vol. 65, no. 10, pp. 1325–1329, 2018.

[49] J. Radic, M. Brkic, A. Djugova, M. Videnovic-Misic, B. Goll, and H. Zimmermann, "Area and power efficient 3–8.8-ghz ir-uwb transmitter with spectrum tunability," *IEEE Microwave and Wireless Components Letters*, vol. 30, no. 1, pp. 39–42, 2019.

[50] Z. Zhang, Y. Li, G. Wang, and Y. Lian, "The design of an energy-efficient ir-uwb transmitter with wide-output swing and sub-microwatt leakage current," *IEEE Transactions on Circuits and Systems II: Express Briefs*, vol. 65, no. 10, pp. 1485–1489, 2018.

[51] A. Uran, K. Ture, C. Aprile, A. Trouillet, F. Fallegger, A. Emami, S. P. Lacour, C. Dehollain, Y. Leblebici, and V. Cevher, "A 16-channel wireless neural recording system-on-chip with cht feature extraction processor in 65nm cmos," in *2021 IEEE Custom Integrated Circuits Conference (CICC)*. IEEE, 2021, pp. 1–2.

[52] A. Omisakin, R. Mestrom, G. Radulov, and M. Bentum, "Sub-milliwatt transceiver ic for transcutaneous communication of an intracortical visual prosthesis," *Electronics*, vol. 11, no. 1, p. 24, 2021.

[53] H. Chen, Z. Chen, R. Ou, R. Chen, Z. Wu, and B. Li, "An ieee 802.15. 4z-compliant reconfigurable pulse-shaping uwb digital power amplifier in 28-nm cmos," *IEEE Transactions on Microwave Theory and Techniques*, 2023.

[54] ——, "A 4-to-9ghz ieee 802.15. 4z-compliant uwb digital transmitter with reconfigurable pulse-shaping in 28nm cmos," in *2022 IEEE Radio Frequency Integrated Circuits Symposium (RFIC)*. IEEE, 2022, pp. 99–102.

[55] Y. Ying, X. Bai, and F. Lin, "A 1-gb/s 6–10-ghz, filterless, pulsed uwb transmitter with symmetrical waveform analysis and generation," *IEEE Transactions on Very Large Scale Integration (VLSI) Systems*, vol. 26, no. 6, pp. 1171–1182, 2018.

[56] W.-S. Choi, M.-C. Park, H.-J. Oh, and Y.-S. Eo, "A switched vco-based cmos uwb transmitter for 3-5 ghz radar and communication systems," *Journal of Semiconductor Technology and Science*, vol. 17, no. 3, pp. 326–332, 2017.

[57] S. Zheng and H. C. Luong, "A cmos wcdma/wlan digital polar transmitter with am replica feedback linearization," *IEEE journal of solid-state circuits*, vol. 48, no. 7, pp. 1701–1709, 2013.

[58] R. Chen, Y. Xiao, Y. Chen, H. Xu, P. Yu, Q. Peng, X. Li, X. Guo, J. Huang, N. Li *et al.*, "A 6.5-to-10ghz ieee 802.15. 4/4z-compliant 1t3r uwb transceiver," in *2022 IEEE International Solid-State Circuits Conference (ISSCC)*, vol. 65. IEEE, 2022, pp. 396–398.

[59] G. de Streel, F. Stas, T. Gurne, F. Durant, C. Frenkel, A. Cathelin, and D. Bol, "Sleeptalker: A ulv 802.15. 4a ir-uwb transmitter soc in 28-nm fdsoi achieving 14 pj/b at 27 mb/s with channel selection based on adaptive fbb and digitally programmable pulse shaping," *IEEE Journal of Solid-State Circuits*, vol. 52, no. 4, pp. 1163–1177, 2017.

[60] E. Allebes, G. Singh, Y. He, E. Tiurin, P. Mateman, M. Ding, J. Dijkhuis, G.-J. Van Schaik, E. Bechthum, J. van den Heuvel *et al.*, "21.2 a 3-to-10ghz 180pj/b ieee802. 15.4 z/4a ir-uwb coherent polar transmitter in 28nm cmos with asynchronous amplitude pulse-shaping and injection-locked phase modulation," in *2021 IEEE International Solid-State Circuits Conference (ISSCC)*, vol. 64. IEEE, 2021, pp. 304–306.

[61] L. Šneler, T. Matić, and M. Herceg, "A tunable cmos ir-uwb pulse generator based on feedback controlled oscillator switching," *IEEE Transactions on Circuits and Systems II: Express Briefs*, vol. 68, no. 6, pp. 1902–1906, 2020.

[62] H. Nikookar and R. Prasad, *Introduction to ultra wideband for wireless communications*. Springer Science & Business Media, 2008.

[63] M. Song, Y. Huang, H. J. Visser, J. Romme, and Y.-H. Liu, "An energy-efficient and high-data-rate ir-uwb transmitter for intracortical neural sensing interfaces," *IEEE journal of solid-state circuits*, vol. 57, no. 12, pp. 3656–3668, 2022.

[64] R. Dong, H. Kanaya, and R. K. Pokharel, "A cmos ultrawideband pulse generator for 3–5 ghz applications," *IEEE Microwave and Wireless Components Letters*, vol. 27, no. 6, pp. 584–586, 2017.

[65] O. Werther, M. Cavin, A. Schneider, R. Renninger, B. Liang, L. Bu, Y. Jin, J. Rogers, and J. Marcincavage, "A fully integrated 14 band, 3.1 to 10.6 ghz 0.13 μm sige bicmos uwb rf transceiver," *IEEE Journal of Solid-State Circuits*, vol. 43, no. 12, pp. 2829–2843, 2008.

[66] H. Hedayati and K. Entesari, "A 90-nm cmos uwb impulse radio transmitter with 30-db in-band notch at ieee 802.11 a system," *IEEE Transactions on Microwave Theory and Techniques*, vol. 61, no. 12, pp. 4220–4232, 2013.

[67] P. P. Mercier, D. C. Daly, and A. P. Chandrakasan, "A 19pj/pulse uwb transmitter with dual capacitively-coupled digital power amplifiers," in *2008 IEEE Radio Frequency Integrated Circuits Symposium*. IEEE, 2008, pp. 47–50.

[68] P. Gunturi, N. W. Emanetoglu, and D. E. Kotecki, "A 250-mb/s data rate ir-uwb transmitter using current-reused technique," *IEEE Transactions on Microwave Theory and Techniques*, vol. 65, no. 11, pp. 4255–4265, 2017.

[69] S. A. Z. Murad, R. K. Pokharel, R. Sapawi, H. Kanaya, and K. Yoshida, "High efficiency, good linearity, and excellent phase linearity of 3.1-4.8 ghz cmos uwb pa with a current-reused technique," *IEEE Transactions on Consumer Electronics*, vol. 56, no. 3, pp. 1241–1246, 2010.

[70] S. Murad, R. Pokharel, A. Galal, R. Sapawi, H. Kanaya, and K. Yoshida, "An excellent gain flatness 3.0–7.0 ghz cmos pa for uwb applications," *IEEE Microwave and Wireless Components Letters*, vol. 20, no. 9, pp. 510–512, 2010.

[71] P. P. Sotiriadis, C. G. Adamopoulos, D. Baxevanakis, P. G. Zarkos, and I. Vassiliou, "Rf switched-capacitor power amplifier modeling," *IEEE Transactions on Computer-Aided Design of Integrated Circuits and Systems*, vol. 40, no. 8, pp. 1525–1530, 2020.

[72] G. Singh, E. Allebes, Y. He, E. Tiurin, P. Mateman, J. F. Dijkhuis, G.-J. van Schaik, E. Bechthum, J. van den Heuvel, M. El Soussi *et al.*, "An ir-uwb ieee 802.15. 4z compatible coherent asynchronous polar transmitter in 28-nm cmos," *IEEE Journal of Solid-State Circuits*, vol. 56, no. 12, pp. 3799–3810, 2021.

[73] S. Gao and K. Moez, "A 2.12-v v_{pp} 11.67-pj/pulse fully integrated uwb pulse generator in 65-nm cmos technology," *IEEE Transactions on Circuits and Systems I: Regular Papers*, vol. 67, no. 3, pp. 1058–1068, 2019.

[74] I. Mahbub, S. Shamsir, S. A. Pullano, and S. K. Islam, "Low-power low-data-rate ir-uwb transmitter for paediatric apnoea monitoring system," *IET Circuits, Devices & Systems*, vol. 13, no. 4, pp. 494–498, 2019.

[75] C. Aprile, K. Ture, L. Baldassarre, M. Shoaran, G. Yilmaz, F. Maloberti, C. Dehollain, Y. Leblebici, and V. Cevher, "Adaptive learning-

based compressive sampling for low-power wireless implants," *IEEE Transactions on Circuits and Systems I: Regular Papers*, vol. 65, no. 11, pp. 3929–3941, 2018.

[76] R. Dong, R. K. Pokharel, H. Kanaya, and K. Yoshida, "Balun with passband characteristic for ultra-wideband (uwb) impulse radio transmitter," in *2012 IEEE Radio and Wireless Symposium*. IEEE, 2012, pp. 323–326.

[77] L. C. Moreira, M. H. Victor, O. Saotome, G. Heck, N. L. Calazans, and F. G. Moraes, "A differential ir-uwb transmitter using pam modulation with adaptive psd," *Analog Integrated Circuits and Signal Processing*, vol. 106, pp. 339–350, 2021.

[78] Z. Zhang, Y. Li, K. Mouthaan, and Y. Lian, "A miniature mode reconfigurable inductorless ir-uwb transmitter–receiver for wireless short-range communication and vital-sign sensing," *IEEE Journal on Emerging and Selected Topics in Circuits and Systems*, vol. 8, no. 2, pp. 294–305, 2018.

[79] P. P. Mercier, D. C. Daly, and A. P. Chandrakasan, "An energy-efficient all-digital uwb transmitter employing dual capacitively-coupled pulse-shaping drivers," *IEEE Journal of Solid-State Circuits*, vol. 44, no. 6, pp. 1679–1688, 2009.

[80] N. Soltani, H. M. Jafari, K. Abdelhalim, H. Kassiri, X. Liu, and R. Genov, "A 21.3%-efficiency clipped-sinusoid uwb impulse radio transmitter with simultaneous inductive powering and data receiving," *IEEE Transactions on Biomedical Circuits and Systems*, vol. 16, no. 6, pp. 1228–1238, 2022.

[81] L. C. Moreira, J. F. Neto, W. A. Van Noije, and S. T. Kofuji, "A ppm gaussian transmitter for uwb using a compact phase detector," in *2011 SBMO/IEEE MTT-S International Microwave and Optoelectronics Conference (IMOC 2011)*. IEEE, 2011, pp. 910–913.

[82] Y. Li, B. Zhou, F. Zhao, Y. Liu, and Y. Jin, "A 1.15-mw low-power low-complexity reconfigurable fm-uwb transmitter," *IEEE Transactions on Very Large Scale Integration (VLSI) Systems*, vol. 30, no. 6, pp. 706–719, 2022.

[83] G. R. Nikandish, A. Nasri, A. Yousefi, A. Zhu, and R. B. Staszewski, "A broadband fully integrated power amplifier using waveform shaping multi-resonance harmonic matching network," *IEEE Transactions on Circuits and Systems I: Regular Papers*, vol. 69, no. 1, pp. 2–15, 2021.

[84] J. Pang, S. He, C. Huang, Z. Dai, C. Li, and J. Peng, "A novel design of concurrent dual-band high efficiency power amplifiers with harmonic control circuits," *IEEE Microwave and Wireless Components Letters*, vol. 26, no. 2, pp. 137–139, 2016.

[85] D. Zito and D. Pepe, "Planar differential antenna design and integration with pulse radar microchip sensor," *IEEE Sensors Journal*, vol. 14, no. 8, pp. 2477–2487, 2014.

[86] M. Särestöniemi, M. Sonkki, S. Myllymäki, and C. Pomalaza-Raez, "Wearable flexible antenna for uwb on-body and implant communications," in *Telecom*, vol. 2, no. 3. MDPI, 2021, pp. 285–301.

[87] X. An, J. Wagner, and F. Ellinger, "An efficient ultrawideband pulse transmitter with automatic on–off functionality for primary radar systems," *IEEE Microwave and Wireless Components Letters*, vol. 30, no. 4, pp. 449–452, 2020.

[88] N. Van Helleputte, M. Verhelst, W. Dehaene, and G. Gielen, "A reconfigurable, 130 nm cmos 108 pj/pulse, fully integrated ir-uwb receiver for communication and precise ranging," *IEEE Journal of Solid-State Circuits*, vol. 45, no. 1, pp. 69–83, 2009.

[89] H. Song, D. Liu, Y. Zhang, W. Rhee, and Z. Wang, "A 6.5–8.1-ghz communication/ranging vwb transceiver for secure wireless connectivity with enhanced bandwidth efficiency and $\delta\sigma$ energy detection," *IEEE Journal of Solid-State Circuits*, vol. 55, no. 2, pp. 219–232, 2019.

[90] E. Bechthum, M. Song, G. Singh, E. Allebes, C. Basetas, P. Boer, A. Breeschoten, S. Cloudt, J. Dijkhuis, M. Ding *et al.*, "A 3-10ghz 21.5 mw/channel rx and 8.9 mw tx ir-uwb 802.15. 4a/z 1t3r transceiver," in *ESSCIRC 2022-IEEE 48th European Solid State Circuits Conference (ESSCIRC)*. IEEE, 2022, pp. 421–424.

[91] H. Song, Z. Ding, W. Rhee, and Z. Wang, "A secure tof-based transceiver with low latency and sub-cm ranging for mobile authentication applications," in *2018 IEEE Radio Frequency Integrated Circuits Symposium (RFIC)*. IEEE, 2018, pp. 160–163.

[92] T. A. Kareem and H. Trabelsi, "Passive mixer-based uwb receiver with low loss, high linearity and noise-cancelling for medical applications," *International Journal of Electronics and Telecommunications*, pp. 61–67, 2023.

[93] N. Shams, A. P. Kakhki, M. Nabavi, and F. Nabki, "An ook and binary fsk reconfigurable dual-band noncoherent ir-uwb receiver supporting ternary signaling," *IEEE Transactions on Very Large Scale Integration (VLSI) Systems*, vol. 31, no. 5, pp. 644–657, 2023.

[94] R. Vauche, E. Muhr, O. Fourquin, S. Bourdel, J. Gaubert, N. Dehaese, S. Meillere, H. Barthelemy, and L. Ouvry, "A 100 mhz prf ir-uwb cmos transceiver with pulse shaping capabilities and peak voltage detector," *IEEE Transactions on Circuits and Systems I: Regular Papers*, vol. 64, no. 6, pp. 1612–1625, 2017.

[95] G. Lee, J. Park, J. Jang, T. Jung, and T. W. Kim, "An ir-uwb cmos transceiver for high-data-rate, low-power, and short-range communication," *IEEE Journal of Solid-State Circuits*, vol. 54, no. 8, pp. 2163–2174, 2019.

[96] O. R. Sparrow, R. Vauché, N. Dehaese, S. Bourdel, J. Gaubert, I. B. Amor, E. Muhr, P. Losco, and O. Fourquin, "High rate uwb cmos transceiver chipset for wban and biomedical applications," *Analog Integrated Circuits and Signal Processing*, vol. 81, pp. 215–227, 2014.

[97] D. B. Issa, M. Hajri, A. Kachouri, M. Samet, and H. Samet, "Reconfigurable uwb transceiver for biomedical sensor application," *BioNanoScience*, vol. 7, pp. 11–25, 2017.

[98] M. Crepaldi, C. Li, J. R. Fernandes, and P. R. Kinget, "An ultra-wideband impulse-radio transceiver chipset using synchronized-ook modulation," *IEEE Journal of Solid-State Circuits*, vol. 46, no. 10, pp. 2284–2299, 2011.

[99] G. Lee, J. Jang, J.-H. Kim, and T. W. Kim, "An ir-uwb cmos transceiver with extended pulse position modulation," *IEEE Journal of Solid-State Circuits*, vol. 57, no. 8, pp. 2281–2291, 2022.

[100] G. Lee, S. Lee, J.-H. Kim, and T. W. Kim, "21.1 a 1.125 gb/s 28mw 2m-radio-range ir-uwb cmos transceiver," in *2021 IEEE International Solid-State Circuits Conference (ISSCC)*, vol. 64. IEEE, 2021, pp. 302–304.

[101] M. Song, Y. Huang, Y. Shen, C. Shi, A. Breeschoten, M. Konijnenburg, H. Visser, J. Romme, B. Dutta, M. S. Alavi *et al.*, "A 1.66 gb/s and 5.8 pj/b transcutaneous ir-uwb telemetry system with hybrid impulse modulation for intracortical brain-computer interfaces," in *2022 IEEE International Solid-State Circuits Conference (ISSCC)*, vol. 65. IEEE, 2022, pp. 394–396.

[102] J. Lei, X. Liu, W. Song, H. Huang, X. Ma, J. Wei, and M. Zhang, "A 1.8 gb/s, 2.3 pj/bit, crystal-less ir-uwb transmitter for neural implants," in *2023 IEEE International Solid-State Circuits Conference (ISSCC)*. IEEE, 2023, pp. 464–466.

[103] M. Crepaldi, G. N. Angotzi, A. Maviglia, F. Diotalevi, and L. Berdondini, "A 5 pj/pulse at 1-gpps pulsed transmitter based on asynchronous logic master–slave pll synthesis," *IEEE Transactions on Circuits and Systems I: Regular Papers*, vol. 65, no. 3, pp. 1096–1109, 2017.

[104] B. Wang, H. Song, W. Rhee, and Z. Wang, "A 7.25-7.75 ghz 5.9 mw uwb transceiver with-23.8 dbm nbi tolerance and 1.5 cm ranging accuracy using uncertain if and pulse-triggered envelope/energy detection," in *2022 IEEE Custom Integrated Circuits Conference (CICC)*. IEEE, 2022, pp. 1–2.

[105] P. P. Mercier, B. H. Calhoun, P.-H. P. Wang, A. Dissanayake, L. Zhang, D. A. Hall, and S. M. Bowers, "Low-power rf wake-up receivers: Analysis, trade-offs, and design," *IEEE Open Journal of the Solid-State Circuits Society*, 2022.

[106] J. Moody, P. Bassirian, A. Roy, N. Liu, N. S. Barker, B. H. Calhoun, and S. M. Bowers, "Interference robust detector-first near-zero power wake-up receiver," *IEEE Journal of Solid-State Circuits*, vol. 54, no. 8, pp. 2149–2162, 2019.

[107] B. Wang, W. Rhee, and Z. Wang, "A quadrature uncertain-if ir-uwb transceiver with twin-ook modulation," in *2023 IEEE International Solid-State Circuits Conference (ISSCC)*. IEEE, 2023, pp. 1–3.

[108] Y. Wei, J. Zhou, Y. Wang, Y. Liu, Q. Liu, J. Luo, C. Wang, F. Ren, and L. Huang, "A review of algorithm & hardware design for ai-based biomedical applications," *IEEE transactions on biomedical circuits and systems*, vol. 14, no. 2, pp. 145–163, 2020.

[109] Z. Fang, W. Wang, J. Wang, B. Liu, K. Tang, L. Lou, C.-H. Heng, C. Wang, and Y. Zheng, "Integrated wideband chip-scale rf transceivers for radar sensing and uwb communications: A survey," *IEEE Circuits and Systems Magazine*, vol. 22, no. 1, pp. 40–76, 2022.

[110] J. Saluja, J. Casanova, and J. Lin, "A supervised machine learning algorithm for heart-rate detection using doppler motion-sensing radar," *IEEE Journal of Electromagnetics, RF and Microwaves in Medicine and Biology*, vol. 4, no. 1, pp. 45–51, 2019.

[111] F. Khan, S. Azou, R. Youssef, P. Morel, and E. Radoi, "Ir-uwb radar-based robust heart rate detection using a deep learning technique intended for vehicular applications," *Electronics*, vol. 11, no. 16, p. 2505, 2022.

[112] A. A. A. Halim, A. M. Andrew, W. A. Mustafa, M. N. Mohd Yasin, M. Jusoh, V. Veeraperumal, M. A. Abd Rahman, N. Zamin, M. R. Mary, and S. Khatun, "Optimized intelligent classifier for early

breast cancer detection using ultra-wide band transceiver," *Diagnostics*, vol. 12, no. 11, p. 2870, 2022.

[113] N. Soltani, H. Kassiri, H. M. Jafari, K. Abdelhalim, and R. Genov, "0.13 μm cmos 230mbps 21pj/b uwb-ir transmitter with 21.3% efficiency," in *ESSCIRC Conference 2015-41st European Solid-State Circuits Conference (ESSCIRC)*. IEEE, 2015, pp. 352–355.

AUTHORS

Razieh Eskandari was born in Urmia, Iran, in 1986. She received the M.Sc. from Urmia University (Urmia, Iran), and Ph.D. in electrical engineering from Sahand University of Technology (Tabriz, Iran) in 2012, and 2020 respectively, both in electronics engineering. She was with Urmia semiconductor company between 2012 and 2015 as a researcher. She joined CenBRAIN Neurotech, Center of Excellence in Biomedical Research on Advanced Integrated-on-chips Neurotechnologies, School of Engineering, Westlake University. Her current research interests include low-power RFIC design and UWB transceivers for biomedical implants and brain-machine interfaces.

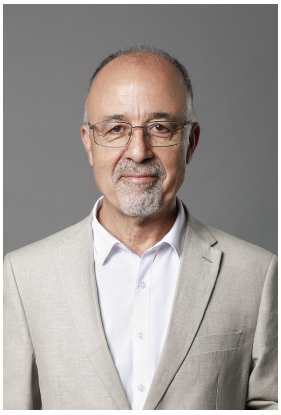

Mohamad Sawan is Chair Professor in Westlake University, Hangzhou, China, and Emeritus Professor in Polytechnique Montreal, Canada. He is the founder and director of the Center of Excellence in Biomedical Research on Advances-on-Chips Neurotechnologies (CenBRAIN Neurotech) in Westlake University, Hangzhou, China, and of the Polystim Neurotech Lab in Polytechnique Montreal. He received his Ph.D. degree from the University of Sherbrooke, Canada. He is Co-Founder, Associate Editor and was Editor-in-Chief of the IEEE Transactions on Biomedical Circuits and Systems (2016-2019). He is the founder of the flagship IEEE International NEWCAS conference and co-founder of the International IEEE-BioCAS and IEEE-AICAS Conferences. He was the General Chair hosting both the 2016 IEEE International Symposium on Circuits and Systems (ISCAS) and the 2020 IEEE International Medicine, Biology and Engineering Conference (EMBC). He was awarded the Canada Research Chair in Smart Medical Devices (2001-2015) and was leading the Microsystems Strategic Alliance of Quebec (ReSMiQ), Canada (1999-2018). Dr. Sawan published more than 1000 peer-reviewed papers, one Handbook, three books, 13 book chapters, and 12 patents, and 20 other patents are pending. He received several awards, among them the most prestigious and first Polytechnique Montreal Research and Innovation Award, the J.A. Bombardier and Jacques-Rousseau Awards from the ACFAS, the Queen Elizabeth II Golden Jubilee Medal, the Medal of Merit from the President of Lebanon, the Barbara Turnbull Award from the Canadian Institutes of Health Research (CIHR), the Shanghai International Collaboration Award, the Zhejiang Westlake Friendship Award, and the Qianjiang Friendship Ambassador Award. Dr. Sawan is a Fellow of the Canadian Academy of Engineering, a Fellow of the Engineering Institutes of Canada, a Fellow of the IEEE, a Fellow of the Asia-Pacific Artificial Intelligence Association (AAIA), and an "Officer" of the National Order of Quebec.